

Nanoscale

Accepted Manuscript



This is an *Accepted Manuscript*, which has been through the Royal Society of Chemistry peer review process and has been accepted for publication.

Accepted Manuscripts are published online shortly after acceptance, before technical editing, formatting and proof reading. Using this free service, authors can make their results available to the community, in citable form, before we publish the edited article. We will replace this *Accepted Manuscript* with the edited and formatted *Advance Article* as soon as it is available.

You can find more information about *Accepted Manuscripts* in the [Information for Authors](#).

Please note that technical editing may introduce minor changes to the text and/or graphics, which may alter content. The journal's standard [Terms & Conditions](#) and the [Ethical guidelines](#) still apply. In no event shall the Royal Society of Chemistry be held responsible for any errors or omissions in this *Accepted Manuscript* or any consequences arising from the use of any information it contains.

COMMUNICATION

Crystalline Phosphorus Fibers: Controllable Synthesis and Visible-Light-Driven Photocatalytic Activity

Cite this: DOI: 10.1039/x0xx00000x

Zhurui Shen,^{a,b} Zhuofeng Hu,^a Wanjun Wang,^a Siu-Fung Lee,^a Donald K. L. Chan,^a Yecheng Li,^a Ting Gu,^a Jimmy C. Yu^{*a}

Received 00th January 2012,

Accepted 00th January 2012

DOI: 10.1039/x0xx00000x

www.rsc.org/

An efficient method has been developed for the synthesis of single crystalline fibrous phosphorus submicron materials. Via the chemical vapor deposition (CVD) technique, fibrous phosphorus fibers with diameters from ~150 nm to 2 μm were prepared directly from amorphous red phosphorus. The as-prepared fibrous phosphorus exhibited interesting photocatalytic properties.

Phosphorus chemistry has drawn enormous attention since the discovery of elemental phosphorus in 1660s.¹ Elemental phosphorus can exist in several forms including the white (P₄), black and red allotropes. Red phosphorus is the most abundant and easily available.² It is stable in ambient conditions and eco-friendly due to its nontoxicity.³ As a result, the applications of red phosphorus have been widespread in our daily life and industry,⁴ such as igniters,^{1a} flame retardant,^{4a} smoke signal^{4b} and chemical analysis^{4c}. Recently, downsizing of phosphorus to submicron or nanoregime has shown numerous fascinating properties in semiconductors,^{5a} rechargeable batteries^{5b,c} and photocatalysts^{5d,e}. For example, red phosphorus/carbon electrode showed a 92 % utilization of phosphorus (equal to 2413 mA.h.g⁻¹) with high columbic efficiencies and cycling stability.^{5b} However, the development of red phosphorus functional materials is still intrinsically limited by the elusive structures of the amorphous red phosphorus.⁶ The fabrication of crystalline red phosphorus, particularly in the form of submicron or nanostructures, is needed to shed light on the definitive correlation of atomic structures with its properties. This may also bring us pleasant surprises for further applications.

It is a hot topic in phosphorus chemistry to resolve the crystalline phase and atomic structures of red phosphorus allotropes.^{2a, 7} Previous works have offered understanding of three kinds of crystalline red phosphorus allotropes. They are type II (hexagonal), type III (unstable) and type V (Hittorf's type).^{2a, 7a-c} Recently, a new member named "fibrous phosphorus (type VI)" has excited the study of phosphorus chemistry and offered a novel kind of potential functional material^{2a, 7f-7h, 8} However, there has been no report on its submicron or nanostructured materials. Moreover, the study of its applications was also in blank. Therefore, it would be interesting to

develop the fibrous phosphorus submicron or nanostructured materials and search their possible applications. Unfortunately, the fabrication of crystalline red phosphorus submicron or nanostructures has been difficult and only type II phosphorus materials have been reported. The synthesis generally required complicated procedures with metallic halides or bismuth as catalysts. Besides that, some toxic reagents were often involved such as potassium cyanide (KCN) or white phosphorus.^{7e, 8} Hence, a safe, economic and controllable preparation method for crystalline red phosphorus submicron or nanomaterials is also necessary.

Herein, we present a "capsule" CVD method for low-cost and controllable synthesis of single crystalline fibrous phosphorus submicron materials. With this method, micron-sized fibrous phosphorus fibers (diameters: 150 nm~2 μm) were obtained. Mechanism analysis showed that the lattice matching between the substrates and products played critical roles for getting the fibrous phosphorus submicron fibers. Moreover, by changing reaction parameters, type II phosphorus submicron rods and Hittorf's phosphorus nanosheets could also be produced. So far, the structure-property relationship of phosphorus materials has only been studied theoretically due to lack of well-defined samples.⁹ Our new method could prepare sufficient amounts of samples easily for investigations. Recently, metal free photocatalysts such as C₃N₄, sulfur and boron etc. have attracted wide interest.¹⁰ This inspired us to study the photocatalytic activity of crystalline phosphorus fibers in this work.

In a typical synthesis, commercial red phosphorus was used as a safe starting material. It was placed in a quartz capsule together with an appropriate substrate (e.g. raw silicon /silicon nanowires wafers, Fig. S1). A vacuum (-0.03~-0.09 Mpa) was maintained before temperature elevation to overcome the kinetic problem of red phosphorus sublimation.^{7f} After gradually cooling to room temperature, fibrous phosphorus submicron materials were obtained on the substrate as confirmed by scanning electron microscopy (SEM) (Fig. 1, Fig. S2).

As shown in Fig. 1 a-c, urchin-like assemblies of submicron fibers were grown on the p-Si (100) nanowires wafers from 100 mg of red phosphorus under an initial pressure of -0.06 Mpa. The submicron fibers were 20-30 μm in length with diameters of 400-600 nm (Fig. 1b, c). Its X-ray diffraction (XRD) pattern (Fig. 1d, Fig. S3) showed

that the reflections were indexed based on space group $P-1(no. 2)$ and consistent with the simulated pattern of triclinic fibrous phosphorus (atomic structure see Fig. 1e, based on crystallographic data CSD 391323).^{7f} The transmission electron microscopy (TEM) analysis was then performed to further resolve its microstructure (Fig. 1f-h, a representative EDX spectrum in Fig. S4). Its high resolution transmission electron microscopy (HRTEM) image (Fig. 1g) displayed clear parallel lattice fringes of (001) facets with a d -spacing of 5.81 Å and (400) facets with a d -spacing of 2.78 Å, which was typical for fibrous phosphorus.^{7f} The selected area electron diffraction (SAED) analysis confirmed its single crystalline nature (Fig. 1h). Although the above analysis demonstrated that the products were mainly single crystalline fibrous phosphorus, we could not fully exclude some unknown impurities grown on the wafer during the complex CVD process. Notably, there were two symmetric groups of spots (highlighted by dot circle) located very close to each other in the SAED pattern. It might be resulted from the stacking atomic layers perpendicular to the incident of electrons, and suggested a layered structure inside. This hypothesis was proved by TEM analysis of broken fibers, which revealed that the layers aligned along the long axis of the fibers (Fig. S5). The HRTEM image further displayed the layers had a d -spacing of 5.67 Å (Fig. S6 inset), which was coincided with the small angle XRD reflection at $2\theta=7.8^\circ$ (twice d -spacing of 11.34 Å, Fig. S6). Based on the X-ray crystallographic analysis, fibrous phosphorus was proposed to have a layered structure stacking by P_{21} pentagonal tubes atomic layers.^{7f} Herein, we characterized this layered structure in detail and confined it into submicron regime.

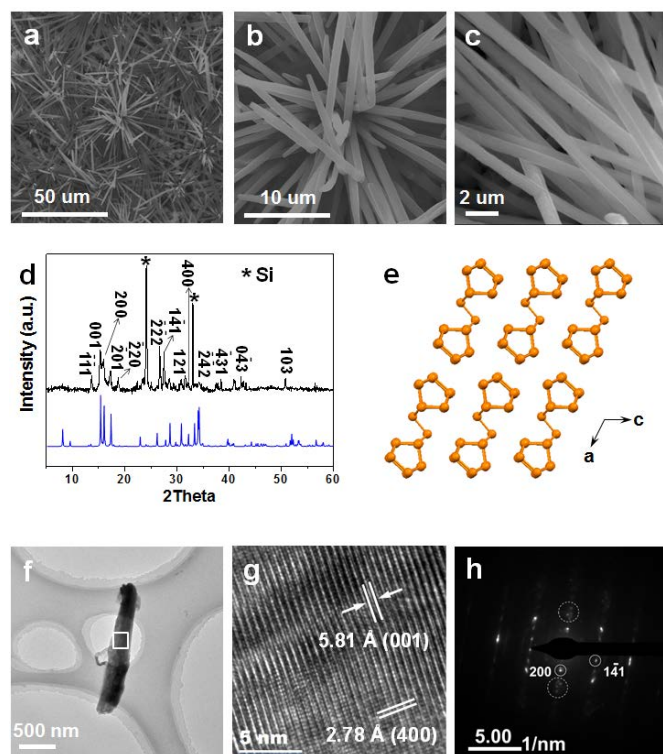


Fig. 1 (a-c) Representative SEM images, (d) XRD patterns, the blue curve was the simulated pattern based on the crystallographic data, (e) Atomic structure and (f-h) TEM, HRTEM and SAED analysis of fibrous phosphorus submicron fibers obtained at -0.06 Mpa, 100 mg red phosphorus and 550 °C.

Moreover, by optimizing the reaction parameters, fibrous phosphorus fibers with variable assembly patterns or diameters could be facially produced (Fig. 2, their XRD patterns in Fig. S7). With the quantity of 100mg red phosphorus and the initial pressure of -0.03 Mpa, the submicron fibers tightly assembled into the dense urchin-like structures but kept similar diameter to ones obtained at -0.06 Mpa (Fig. 2a). When the initial pressure decreased to -0.09 Mpa, the dense assemblies became very few, and dispersed submicron fibers dominated the final products (Fig. 2b). A mechanism (Scheme S1) was proposed to explain this pressure controlled growth. When the quantity of red phosphorus was reduced to 50 mg, the diameter of submicron fibers was greatly decreased to ~150 nm, which was only 25 % of that obtained with 100 mg precursor (Fig. 2c). While using 150 mg red phosphorus, the diameter of products was enlarged to ~2 μm and shuttle like microfibers were produced (Fig. 2d). These fibrous phosphorus fibers were found to contain the same layered structure (Fig. S8a-d).

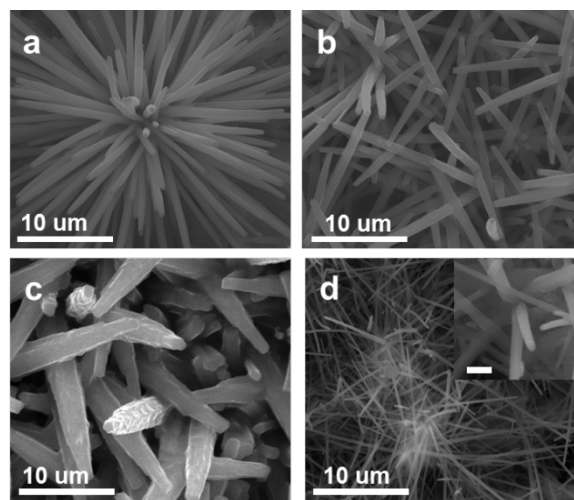


Fig. 2 Representative SEM images of fibrous phosphorus submicron and microfibers obtained at (a)-0.03 Mpa, 100mg red phosphorus, (b) -0.09 Mpa, 100 mg red phosphorus, (c) -0.06 Mpa, 50 mg red phosphorus and (d) -0.06 Mpa, 150 mg red phosphorus, the scale bar is 500 nm in the inset picture of (c). The reaction temperature is 550 °C.

To illustrate the formation mechanism of fibrous phosphorus submicron fibers, the lattice matching effect between fibrous phosphorus and substrates was demonstrated here as the potential key factor for its controllable growth. As shown in Fig. 3a, the p-Si (100) wafer ($Fd-3m (227)$) displayed a lattice fringe constant of 5.43 Å for (001) and (010) facets. Hence, it well matched with the interlayer spacing of 5.67 Å for fibrous phosphorus submicron fibers, and thus induced an energetically favorable growth along the long axis of fibers (Fig. S5).¹¹ Besides that, a crucial step of lattice matching growth (or epitaxial growth) in CVD is the stress relaxation in crystals.^{11d,e} Fibrous phosphorus is a kind of molecular crystal connected by weak van der Waals forces, which might be also beneficial for its stress relaxation during the crystal growth. To further verify the lattice matching effect, other substrates were also studied here. When using p-Si (111) nanowires wafer, which showed no obvious lattice match relationship with red phosphorus allotropes. Only a mixture of fibrous phosphorus submicron fibers and type II phosphorus submicron rods⁸ was obtained on the substrate. It

suggested an uncontrolled crystal growth and further proved the role of lattice matching effect (Fig. 3b, c and XRD pattern in Fig. S9a). Additionally, similar fibrous phosphorus submicron fibers were produced on n-Si (100) nanowires wafer and plain p-Si (100) wafer. (Fig. 3d, e and XRD patterns in Fig. S9b, c). However, their assembly patterns on the plain Si wafer were not as obvious as those on the Si nanowires wafer. This might be due to the influence of a rough surface on the nucleation process. A dynamic growth process for the fibrous phosphorus is proposed in Scheme S2.

Besides the fibrous phosphorus, other red phosphorus allotropes could also be obtained via this method. When using α -Ti wafer as the growing substrate (100 mg red phosphorus, -0.06 Mpa), type II phosphorus submicron rods with length of 3-5 μm and diameter of 300-400 nm were produced (Fig. S10a, b and Fig. S11a).⁸ In the previous study, type II phosphorus was defined as a crystalline allotrope of red phosphorus by TGA analysis (stable in the range of 460-520 $^{\circ}\text{C}$).^{2a} Recently, Winchester *et al.* have shown the only example of type II phosphorus nanostructures prepared with white phosphorus as the starting material.⁸ Herein, our method offered a safe way to get type II phosphorus submicron rods. While on the p-Si (100) nanowires wafer, Hittorf's phosphorus nanosheets could be obtained under the reaction temperature of 450 $^{\circ}\text{C}$ (Fig. S10c, d and Fig. S11b). These examples showed that our method was a general protocol for obtaining crystalline red phosphorus allotropes submicron and nanostructures.

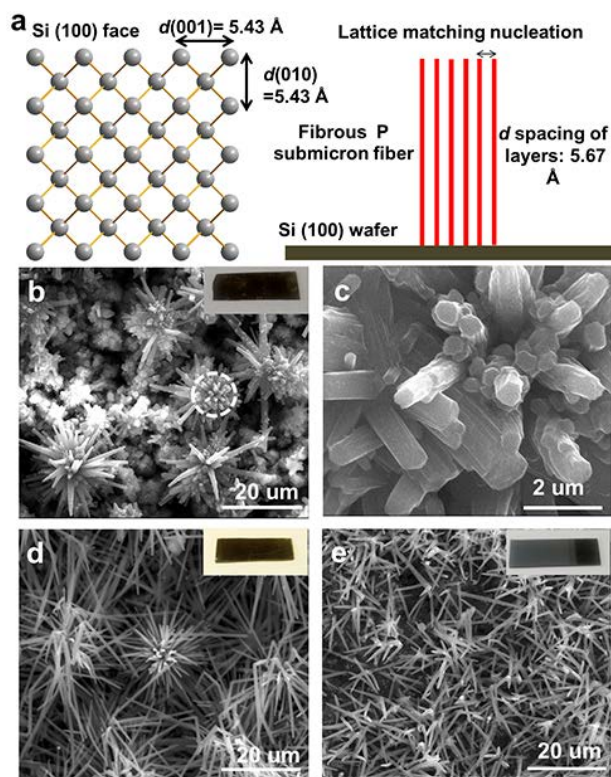


Fig. 3 (a) The illustration of lattice matching effect of fibrous phosphorus submicron fibers vs. p-Si (100) nanowires wafer. Red phosphorus submicron materials obtained on (b, c) p-Si (111) nanowires wafer, (d) n-Si (100) nanowires wafer and (e) bare p-Si (100) wafer at -0.06 Mpa, 100 mg red phosphorus and 550 $^{\circ}\text{C}$. Picture (c) was the highlighted zone in (b). "P": phosphorus.

The as-prepared fibrous phosphorus submicron fibers displayed interesting visible light driven photocatalytic activity, in addition, the photocatalytic property of type II phosphorus submicron rods was also studied here for comparison (Fig. 4). Photocurrent response under visible light irradiation ($\lambda > 420 \text{ nm}$) was firstly test, and their obvious on-off photocurrents verified that electrons and holes could be generated over red phosphorus allotropes (Fig. S12). Thereafter, degradation of Rhodamine B (RhB) under visible light ($\lambda > 420 \text{ nm}$) was performed as the model experiment. As shown in Fig. 4a, the RhB degradation efficiencies over fibrous phosphorus submicron fibers (sample see Fig. 1a-c) and type II phosphorus submicron rods (sample see Fig. S10a, b) were 46.4 % and 28.8 % (23.2 %/ mg of catalyst and 14.4%/ mg of catalyst), respectively, under visible light irradiation for 6 h (c.a. 2 mg catalyst/ 20 mL solution; silicon nanowires wafer showed no photocatalytic activity, Fig. S13). Fibrous phosphorus submicron fibers showed a ~ 1.6 times of apparent reaction rate (normalized with the area of wafers) than type II phosphorus submicron rods. Considering the larger size of former one, fibrous phosphorus should have higher intrinsic photocatalytic activity than type II phosphorus. This difference could be understood from two aspects. For one thing, fibrous phosphorus submicron fibers had a wider visible light absorption of $\sim 100 \text{ nm}$ than type II phosphorus submicron rods (Fig. 4b), which originated from their different crystalline phase and thus electronic structure. For another, the layered structure of fibrous phosphorus was favorable for the separation of photo-generated electrons and holes. Anisotropic transport behaviors of photo-generated electrons and holes in the layered photocatalysts have been evidenced in other systems.¹² While the small angle XRD analysis showed that there was no layered structure in type II phosphorus (Fig. S8e). The stability of fibrous phosphorus as the photocatalyst was also evaluated here, and its activity was virtually unchanged after three cycles (Fig. S14). Their OH radical detections were also performed, and the increasing fluorescence intensities confirmed the involvement of OH radicals in the photocatalytic pathway (Fig. 4 c, d).

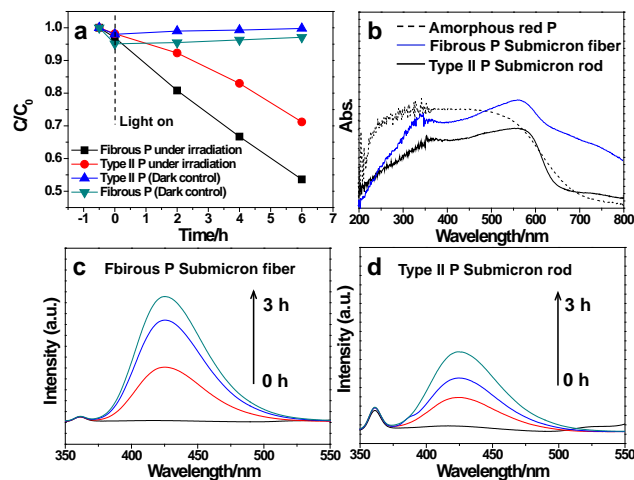


Fig. 4 (a) Photocatalytic performance of fibrous phosphorus submicron fibers vs. type II phosphorus submicron rods, via the degradation of RhB under visible light irradiation. (b) Their UV-vis diffuse reflectance spectra, the spectrum of amorphous red phosphorus was used as the reference. (c, d) Their time dependent fluorescence spectra of the terephthalic acid solution ($4 \times 10^{-4} \text{ M}$), each fluorescence spectrum was recorded every 1 hour of visible light illumination.

Moreover, colorless 2, 3, 6-trichlorophenol was also degraded over the fibrous phosphorus submicron fibers, and showed a reduction of 41.9 % after 6 h irradiation of VL (Fig. S15). In addition, amorphous red phosphorus nanoparticle was used to degrade the RhB under VL irradiation and compared with fibrous phosphorus fibers powder. It is shown that (Fig. S16, 2 mg catalyst), after 4 h irradiation, the degradation efficiency of RhB over red P nanoparticle and fibrous phosphorus fibers was 54.5 % and 86.3 %, respectively. These results suggested that the crystalline structure of fibrous phosphorus might be beneficial for its activity due to some possible advantages e.g. fast charge separation.

Conclusions

In summary, single crystalline fibrous phosphorus submicron fibers/microfibers have been realized via a “capsule” CVD method. The lattice matching effect between the substrate and phosphorus was found critical for obtaining desired product. Moreover, type II phosphorus submicron rods and Hittrof’s phosphorus nanosheets could also be fabricated using this method. Our method does not require catalysts or mineralizers, and it is relatively low cost. The facile control of morphology and crystalline phase make this method a general protocol for red phosphorus and other potential sublimating elements such as sulfur and arsenic. Moreover, photocatalytic activity of fibrous phosphorus and type II phosphorus was evaluated here and showed obvious phase-dependent behavior, which would provide inspirations for their further applications in many other fields e.g. battery electrodes or supercapacitors.

Acknowledgements

This work was partially supported by the Shenzhen Basic Research Scheme (JCYJ20120619151417947) and a grant from the Research Grants Council of the Hong Kong Special Administrative Region, China, under Theme-based Research Scheme through Project No. T23-407/13-N. The authors are grateful to Prof. Gang Liu (IMR, CAS, China) for helpful discussion.

Notes and references

^a Department of Chemistry, The Chinese University of Hong Kong, Shatin, New Territories, Hong Kong, China & Shenzhen Research Institute, The Chinese University of Hong Kong, Shenzhen, China.

^b Key Laboratory for Advanced Ceramics and Machining Technology of Ministry of Education, Tianjin University & School of material Science and Engineering, Tianjin University, Tianjin 300072, China.

Electronic Supplementary Information (ESI) available: [Experimental sections and other supporting characterization data.] See DOI: 10.1039/c000000x/

- (a) M. Scheer, G. Balázs and A. Seitz, *Chem. Rev.* 2010, **110**, 4236; (b) J. R. Nitschke, *Nat. Chem.* 2011, **3**, 90; (c) E. E. Coyle and C. J. O’Brien, *Nat. Chem.* 2012, **4**, 779.
- (a) W. L. Roth, T. W. Dewitt and A. J. Smith, *J. Am. Chem. Soc.* 1947, **69**, 2881; (b) M. Ceppatelli, R. Bini, M. Caporali and M. Peruzzini, *Angew. Chem. Int. Ed.* 2013, **52**, 2313.
- J. A. Young, *J. Chem. Educ.*, 2004, **81**, 945.
- (a) U. Braun and B. Schartel, *Macromol. Chem. Phys.* 2004, **205**, 2185; (b) E. C. Koch, *Propell. Explos. Pyrot.* 2008, **33**, 165; (c) J. Havel, *Rapid Commun. Mass Spectrom.* 2009, **23**, 3114.
- (a) S. Mahapatra, H. Ryu, S. Lee, A. Fuhrer, T. C. G. Reusch, D. L. Thompson, W. C. T. Lee, G. Klimeck, L. C. L. Hollenberg and M. Y. Simmons, *Science* 2012, **335**, 64; (b) Wang, L. et al. *Angew. Chem. Int. Ed.* 2012, **51**, 9034; (c) Kim, Y. J. et al. *Adv. Mater.* 2013, **25**, 3045; (d) Wang, F. et al. *Appl. Catal. B: Environ.* 2012, **111-112**, 409; (e) Wang, F. et al. *Appl. Catal. B: Environ.* 2012, **119-120**, 267.
- J. M. Zaug, A. K. Soper and S. M. Clark, *Nat. Mater.* 2008, **7**, 890.
- (a) V. H. Thurn and H. Krebs, *Acta Cryst. B.* 1969, **25**, 125; (b) M. E. Barr, *J. Am. Chem. Soc.* 1991, **113**, 3052; (c) M. Häser, *J. Am. Chem. Soc.* 1994, **116**, 6925; (d) H. Hartl, *Angew. Chem. Int. Ed.* 1995, **34**, 2637; (e) A. Pfitzner, M. F. Bräu, J. Zweck, G. Brunklaus and H. Eckert, *Angew. Chem. Int. Ed.* 2004, **43**, 4228; (f) M. Ruck, D. Hoppe, B. Wahl, P. Simon, Y. K. Wang and G. Seifert, *Angew. Chem. Int. Ed.* 2005, **44**, 7616; (g) S. Lange, M. Bawohl, R. Wehrich and T. Nilges, *Angew. Chem. Int. Ed.* 2008, **47**, 5654. (h) N. Eckstein, A. Hohmann, R. Wehrich, T. Nilges and P. Schmidt, *Z. Anorg. Allg. Chem.* 2013, **639**, 2741.
- R. A. L. Winchester, M. Whitby and M. S. P. Shaffer, *Angew. Chem. Int. Ed.* 2009, **48**, 3616.
- (a) G. Seifert and E. Hernández, *Chem. Phys. Lett.* 2000, **318**, 355; (b) D. W. Drumm, J. S. Smith, M. C. Per, A. Budi, L. C. L. Hollenberg and S. P. Russo, *Phys. Rev. Lett.* 2013, **110**, 126802.
- (a) X. H. Li, X. C. Wang and M. Antonietti, *Chem. Sci.* 2012, **3**, 2170; (b) G. Liu, P. Niu, C. H. Sun, S. C. Smith, Z. G. Chen, G. Q. Lu and H. M. Cheng, *J. Am. Chem. Soc.* 2010, **132**, 11642; (c) G. Liu, P. Niu, L. C. Yin and H. M. Cheng, *J. Am. Chem. Soc.* 2012, **134**, 9070; (d) G. Liu, L. C. Yin P. Niu, W. Jiao and H. M. Cheng, *Angew. Chem. Int. Ed.* 2013, **52**, 6242.
- (a) E. C. Nelson, et al. *Nat. Mater.* 2011, **10**, 67; (b) Yang, W. et al. *Nat. Mater.* 2013, **12**, 792; (c) C. Zhen, G. Liu and H. M. Cheng, *Nanoscale* 2012, **4**, 3871; (d) E. R. Buß, U. Rossow, H. Bremers and A. Hangleiter, *Appl. Phys. Lett.* 2014, **104**, 162104; (e) K. Lorenz, N. Franco, E. Alves, S. Pereira, I. M. Watson, R. W. Martin and K. P. O’Donnell, *J. Cryst. Growth* 2008, **310**, 4058.
- (a) Y. Matsumoto, S. Ida and T. Inoue, *J. Phys. Chem. C* 2008, **112**, 11609; (b) G. Liu, et al. *J. Mater. Chem.* 2010, **20**, 831. (c) J. Jiang, K. Zhao, X. Y. Xiao and L. Z. Zhang, *J. Am. Chem. Soc.* 2012, **134**, 4473.